Tutors

Dr. Ángel Morales García
Departament de Ciència de Materials i Química Física

Dr. Francesc Viñes Solana
Departament de Ciència de Materials i Química Física

Grau de Química

Treball Final de Grau

Single-Atom Catalysts Based on O-Functionalized MXenes

Catalitzadors d'àtoms aïllats suportats a MXenes funcionalitzats amb oxigen

Maria Andreea Buturca

January 2022

Universitat de Barcelona

B:KC Barcelona Knowledge Campus
Campus d'Excel·lència Internacional

You know the best thing about a scientist is also the worst thing:

they are always working

Iron Man

En primer lloc, m'agradaria agrair als meus dos tutors, Fransis i Ángel per haver fet aquest camí més amè i per la seva paciència. Tot i ser un tema inicialment molt complicat per a mi, han aconseguit que arribi a agradar-me molt el que hem fet en aquest treball.

També vull fer especial esment a la meva parella i al meu millor amic, que han estat els que m'han acompanyat en els moments bons i no tan bons al llarg d'aquest treball final i de tota la carrera.

REPORT

CONTENTS

1. SUMMARY 3
2. RESUM 5
3. INTRODUCTION 7
4. OBJECTIVES 11
5. THEORETICAL BACKGROUND 13
5.1. Quantum Chemistry 13
5.1.1. The Schrodinger equation and Born-Oppenheimer approximation 13
5.1.2. Density functional theory 14
5.1.3. Exchange-correlation energy 16
5.2. Computational Models 17
5.2.1. Periodic model 18
5.3. MXenes 19
5.3.1. Single atom positions 21
5.4. Single Atom Energy Assessment 21
5.4.1. Adsorption energy 21
5.4.2. Cohesive energy 22
6. COMPUTATIONAL DETAILS 23
7. RESULTS AND DISCUSSION 25
7.1. TM@MXenes: Site and Stability 25
7.2. TM@MXenes: Adsorption Energies 25
7.2.1. Adsorption energies of 4*d* adatoms 26
7.2.2. Heights of TM adatoms with respect M_2CO_2 for the 4*d* series 27
7.2.3. Isolating or clustering trends for 4*d* TMs 30
7.2.4. Adsorption energies of 5*d* TMs 32
7.2.5. Heights of TM adatoms with respect M_2CO_2 for the 5*d* series 33
7.2.6. Isolating or clustering trends for 5*d* TMs 35

7.2.7. Different series comparison 37
7.3. Diffusion Aspects 39
8. CONCLUSIONS 43
9. REFERENCES 45

1. SUMMARY

Single-atom catalysts (SACs) are the maximal expression of nanostructuring, of vital importance to maximize the efficiency of late, scarce, and expensive transition metals (TMs), regularly used as catalysts for a large variety of industrial chemical applications. SACs are fundamentally determined by their stability, where proper substrates that disperse them are key. Focusing on these, two-dimensional (2D) transition metal carbides, nitrides, and carbonitrides, known as MXenes, have gained much interest due to their inherent 2D nature, which suggests them as a suitable platform for disperse TM adatoms. Here we study, by density functional theory (DFT), the TM single-atom adsorption energy and stability for 4*d* and 5*d* TMs on nine O-functionalized MXenes with stoichiometry M_2CO_2 (M = Ti, Zr, Hf, V, Nb, Ta, Cr, Mo, and W), reliable models according to experimental evidences. The TM adsorption sites and heights are identified, analyzing adsorption energy trends along the *d* series, as well the MXene groups and series, identifying that the adsorption strengths decay along the *d* series, and are highly influenced by the TM stability, where especially stable d^5 and d^{10} configurations show the smallest adsorption energies. Aside, the adsorption strength increases along the MXene series, but decays down the MXene groups. SACs are found to be energetically favorable for early and late TMs, and specially enhanced on V_2CO_2, Cr_2CO_2, Mo_2CO_2, and W_2CO_2 MXenes, although dispersion and/or aggregation can be affected by the TM adatom diffusion energy barriers.

Keywords: O-Functionalized MXenes, Density Functional Theory, Single-Atom Catalysts, Adsorption Energies, Diffusion.

2. RESUM

Els catalitzadors d'àtoms aïllats (en anglès, *single-atom catalysts* o SACs) són la màxima expressió de la nanoestructuració, de vital importància per maximitzar l'eficiència dels metalls de transició (*transition metals* - TMs) tardans, escassos i cars, utilitzats de manera regular com a catalitzadors per a una gran varietat de reaccions químiques d'interés industrial. Els SACs estan fonamentalment determinats per la seva estabilitat, on els substrats adequats que els dispersen són clau. Centrant-nos en aquests, els carburs, nitrurs i carbonitrurs de metalls de transició bidimensionals (2D), coneguts com a MXenes, han guanyat molt interès gràcies a la seva naturalesa 2D inherent que els suggereix com una plataforma adequada per dispersar adàtoms de TM. Aquí estudiem, mitjançant la teoria funcional de la densitat (*density functional theory* - DFT) en models adequats de llesca (*slab*) de superfície MXenes, l'energia d'adsorció i estabilitat d'àtoms aïllats de metalls 4*d* i 5*d* en nou MXenes funcionalitats amb oxigen amb estequiometria M_2CO_2 (M = Ti, Zr, Hf, V, Nb, Ta, Cr, Mo, i W), considerant que aquestes terminacions dels MXenes es poden aconseguir experimentalment d'una manera realista. Els llocs d'adsorció i alçades dels TM s'han identificat, analitzant les tendències d'energia d'adsorció al llarg de les sèries *d*, així com els grups i sèries dels MXenes, identificant que les forces d'adsorció decauen al llarg de les sèries *d*, i que estan fortament influenciades per l'estabilitat dels TM, on les configuracions especialment estables d^5 i d^{10} mostren les energies d'adsorció més petites. A part, la força d'adsorció augmenta al llarg de la sèrie dels MXenes, però decau al llarg dels grups dels MXenes. Els SACs són energèticament favorables per a TMs del principi i final de la sèrie *d*, especialment en els MXenes de V_2CO_2, Cr_2CO_2, Mo_2CO_2 i W_2CO_2, encara que la dispersió i/o agregació pot estar afectada per la barrera de difusió dels TMs.

Paraules clau: MXenes funcionalitzats amb oxigen, Teoria funcional de la densitat, Catalitzadors d'àtoms aïllats, Energies d'adsorció, Difusió

3. INTRODUCTION

The term Catalysis could be defined as the improvement of a given chemical reaction process by the mere presence of a catalyst. A catalyst is simply a compound that helps transforming reactants into products, typically in a faster way, and so implying a lower consumption of energy. Generally, it is stated that a catalyst reduces the reaction energy barriers, making the production faster, and so, requiring less energy to reach the sought production rates. Notice that, apart from speeding up the chemical reaction, an ideal catalyst is not consumed during the process, this is, it is not a reactant, and indeed is able to participate in a new catalytic cycle once products are created and released. Note that catalysts may simply imply a selectivity improvement over a rate acceleration; this is again achieved by lowering barriers of a certain, sought product, while raising the ones of the other, undesired products. Catalysts play a large, key role in industry, since, currently, catalysts are involved in 90% of the existing chemical processes,[1] and account for more than 37% of the gross domestic product (GDP).[2]

Depending on the phasic nature or reactants and the catalyst, the latter can be classified as homogeneous or heterogeneous. In the former, the catalyst species work in the same physic (or phasic) state as the reagents, thus being very effective thanks to the ease of movement and capabilities of reaching reagents, but, on the other part, they tend to be not very reusable or stable, and require separation steps of products from the catalyst. The heterogeneous catalysts are normally conformed by a solid substrate where the reactants are adsorbed on, transformed into products, and finally products get desorbed. Heterogeneous catalysts are the most used in the industry, particularly, as they allow for a rapid separation of products from catalyst, allowing for continuous *operando* conditions, and are normally quite stable during the reaction.

Nowadays there are worldwide research endeavors placed at finding new and improved catalyst, so as to reduce the energy usage, as a key requirement in circular energy, and by that, contributing at reducing greenhouse gases emissions.[3] Nanostructuring catalyst, *e.g.* using nanoparticles, has been conceptualized as a way of increasing the amount of the catalyst material in contact with reagents, and so, maximizing their efficiency. One of the most active

applications in Heterogeneous Catalysis nowadays is driving nanostructuring to its limit, this is, the use of single atom catalysts (SACs).

The concept of SACs in Catalysis was firstly introduced in 2011 by Zang and collaborators when they prepared a Pt_1/FeO_x SAC for carbon monoxide (CO) oxidation towards carbon dioxide (CO_2).[4] They observed greater activity, stability, and selectivity when the Pt metal was dispersed as individual atoms at low temperatures, where such single-atom sites were used as active sites.[4] SACs are thus described as isolated atoms (typically noble or non-noble transition metals) anchored to a support by a chemical bond or a stable metal-support interaction. Indeed, such atoms can be present as adsorbed atoms (adatoms), although they can be present at the surface as a solid solution site within the substrate, seen, *e.g.* for doping quantities of a metal within another metal substrate.[5] The size reduction of such metallic active phases constitutes a great advantage when determining the catalytic performance, especially for scarce and expensive late transition metals (TMs) such as Ir, Os, Ru, Rh, Pd and Pt, known as Pt-group metals, which are commonly the catalytic active phases in many reactions of pharmaceutical and petrochemical industries, as well as in environmental protection processes. Even if these metals performance is quite high, their use is limited due to their high cost and low natural abundance,[6] and is just because of that catalysts of Earth-abundant lower cost and higher activities are urgently needed for large-scale applications, although another way of approaching the problem is simply maximizing these TMs efficiency.

A fundamental, key aspect of SACs is the selection of appropriate substrates where adatoms are anchored and dispersed. Ideally, such materials must display large surface areas, and strongly attach the TM adatoms. To this end, different two-dimensional (2D) materials have been explored, including graphene,[7] graphynes,[8] hexagonal boron nitride (*h*-BN), transition metal dichalcogenides (TMDs), germanene, phosphorene, silicene, etc, generally revealing that SACs are stabilized either at materials native defects, *e.g.* vacancies or low-coordinated sites, or on regular sites of metastable materials, as highlighted by different computational simulations, mostly based on density functional theory (DFT).[9] Recently, a new kind of 2D layered early transition metal carbide, nitride, and carbonitride materials, known as MXenes, have been obtained by the selective chemical etching of MAX phases. MAX forms generally have the following formula: $M_{n+1}AX_n$ (n=1–3) where *M* represents an early TM, *A* stands for a *p*-

block element, and *X* represents C or N. The ability of these materials to form carbonitrides and other metal solid solutions gives rise to an infinite number of different compositions, opening the doors to new atomistic designs.[9] It has been seen that the bare MXenes sheets surfaces are chemically very active, and tend to be surface terminated by O, OH, or F moieties, as a result of the MAX etching process, generally carried out using hydrofluoric acid (HF).[10] Notice that there exist F-free treatments with only O and OH terminations,[11] and that at high temperatures the OH group transform into O. This is why MXenes terminated by O-groups are thought to be more easily prepared.[11] Such materials have been shown to be ideal candidates as substrates for Li-based batteries,[12] interesting sensors for organic compounds,[13,14] or even to be used as electromagnetic shields.[15] Following a previous study where 3*d* TM adatoms stability was explored on a set of MXenes, the goal of the present project is to analyze, by DFT means on suitable models, the 4*d* (Y, Zr, Nb, Mo, Tc, Ru, Rh, Pd, Ag and Cd) and 5*d* (Hf, Ta, W, Re, Os, Ir, Pt, Au, and Hg) TM adatoms stability on M_2CO_2 MXene models, with M being Ti, Zr, Hf, V, Nb, Ta, Cr, Mo, and W, see Figure 1.

H																	He
Li	Be											B	C	N	O	F	Ne
Na	Mg											Al	Si	P	S	Cl	Ar
K	Ca	Sc	Ti	V	Cr	Mn	Fe	Co	Ni	Cu	Zn	Ga	Ge	As	Se	Br	Kr
Rb	Sr	Y	Zr	Nb	Mo	Tc	Ru	Rh	Pd	Ag	Cd	In	Sn	Sb	Te	I	Xe
Cs	Ba	La	Hf	Ta	W	Re	Os	Ir	Pt	Au	Hg	Tl	Pb	Bi	Po	At	Rn
Fr	Ra	Lr	Rf	Db	Sg	Bh	Hs	Mt	Ds	Rh	Cn	Nh	Fl	Mc	Lv	Ts	Os

Figure 1. Periodic Table representation where *M* metals are highlighted in blue, TM adatoms in gray, *X* (C) in brown, and surface termination (O), in red.

4. OBJECTIVES

The main objective of this work is to systematically study the behavior and capacity of O-terminated C-based MXenes with the M_2CO_2 stoichiometric formula (M = Ti, Zr, Hf, V, Nb, Ta, Cr, Mo, and W) as supports and dispersants of single transition metal (TM) adatoms from 4*d* (Y, Zr, Nb, Mo, Tc, Ru, Rh, Pd, Ag, and Cd) and 5*d* (Hf, Ta, W, Re, Os, Ir, Pt, Au, and Hg) series, so as to evaluate their substrate possibilities for single atom catalysts (SACs). Based on this idea, the following goals will be analyzed and discussed:

- Find most stable sites for the 4*d* and 5*d* TMs on the nine explored M_2CO_2, and the adsorption strengths.
- Evaluate trends of their adsorption energies along the 4*d* and 5*d* series, as well as along the M_2CO_2 M series and groups.
- Correlate the adsorption heights with the adsorption energies, and identify physisorption and chemisorption situations.
- Forecast the single-atom energetic stability by comparing the adsorption energy strength with the 4*d* or 5*d* TM bulk cohesive energy, and identify trends along *d*-series and M_2CO_2 series and groups.
- For some exemplary cases, evaluate the impact of the single adatom diffusion energy barrier on their isolation or clustering.

5. THEORETICAL BACKGROUND

5.1. QUANTUM CHEMISTRY

Quantum Chemistry is the application of quantum physics or quantum mechanics to chemical systems; and since it derives from it, it constitutes as well one of the greatest advances in Science of the 20th century. Specifically, it grounds in the description of the nature and interaction of atomic and subatomic systems at the atomic scale, where the system properties are not consistent with the expected behavior observed on the macroscopic world, and ruled by classical physics. In short, one can state that Newton's laws describe classical mechanics, whereas Schrödinger equation (see below) is the most relevant equation to quantum mechanics. The explanation of matrix mechanics by Heisenberg and wave mechanics by Schrödinger, which turned out to be equivalent, ended up paving the way for nowadays Quantum Mechanics, which is briefly described next.

5.1.1. The Schrödinger equation and Born-Oppenheimer approximation

The time-independent Schrödinger equation (Eq. 1) implies that, for a system described by a wavefunction Ψ, one can apply the Hamiltonian on it, $\hat{\mathrm{H}}$, and get the system energy, *E*. For this reason, during the last century, great efforts were devoted to solving this equation achieving the highest accuracy possible.

$$\hat{\mathrm{H}}\Psi = E\Psi \quad (1).$$

The Hamiltonian can be separated into different types of operators, including $\hat{T}$, describing the kinetic energies, and $\hat{V}$, describing the potential energies, or, in other words, the coulombic interactions:

$$\hat{\mathrm{H}}\Psi = \left(\hat{T} + \hat{V}\right)\Psi \quad (2).$$

Furthermore, the $\hat{T}$ and $\hat{V}$ operators can be separated depending on whether they describe properties of electrons, *e*, nuclei, *n*, or between nuclei and electrons.

$$\hat{\mathrm{H}}\Psi = \left(\hat{T}_e + \hat{T}_n + \hat{V}_{ee} + \hat{V}_{nn} + \hat{V}_{en}\right)\Psi \quad (3),$$

where $\hat{T}_e$ corresponds to the kinetic energy of the electrons, $\hat{T}_n$ is the kinetic energy of the nuclei, $\hat{V}_{ee}$ corresponds to the coulombic repulsion between electrons, $\hat{V}_{nn}$ is the coulombic repulsion in between nuclei, and $\hat{V}_{en}$ describes the coulombic attraction between nuclei and electrons.[16] Although at first glance it does not seem a complex equation, the time-independent Schrödinger equation is very difficult to calculate, being analytically only possible for systems with one nucleus and one electron —called hydrogenoid atoms, such as H atom, or Li^+ cation—, but it is unfeasible for other systems, which have to be approximated.

The first and more basic approximation is that of Born-Oppenheimer Approach (BOA),[17] which is key in Quantum Chemistry. It is based on the fact that the relative mass of the electrons is much smaller than that of nuclei, so the movement of the nuclei does not condition the kinetic energy of the electrons, and $\hat{V}_{nn}$ can be considered a constant, while $\hat{T}_n$ can be considered zero. Thus, one solves the electronic Schrodinger equation at fixed internuclear distances, using the electronic Hamiltonian, $\hat{\mathrm{H}}_e$:

$$\hat{\mathrm{H}}_e\Psi = \left(\hat{T}_e + +\hat{V}_{ee} + +\hat{V}_{en}\right)\Psi \qquad (4).$$

This allows studying a molecular structure separated into two distinct stages, but without being a separable system:

- One first solves the electronic part considering that the nuclei have fixed positions, obtaining an electronic surface potential energy.
- One later solves the nuclear movement problem on the solution generated in the first stage.

This scheme can be followed iteratively until convergence, but there is still another problem to be solved related the electronic correlation for multielectronic systems. Different methods have been developed to account for this correlation, known as post-Hartree-Fock (HF) methods, although a popular approach to account for correlation while being computational affordable is density functional theory (DFT), explained next.

5.1.2. Density functional theory

To forge the basis of DFT, we must rely on the two theorems derived by Hohenberg and Kohn.[18] The first theorem shows that there is a relationship between the external potential, *i.e.* the coulombic potential generated by the atoms nuclei, and the electron density for the ground

state, $\rho_0(r)$, meaning that, except by differing from a constant, the ground state electron density cannot come from two different external potentials. To put it plainly, the nuclei positions and charges define how the electron density is best arranged around them, and *vice versa*. The second theorem determines that the system ground state energy, E_0, can be expressed as a function of the electron density function, $\rho(r)$, this is, a functional of the electron density, and that the ground state electron density, $\rho_0(r)$, minimizes the system energy,[19] and so, this can be achieved variationally.

$$E_0 = E_0[\rho(r)] \quad (5).$$

The main advantage of DFT over HF and post-HF methods is that the latter require knowing the spatial coordinates —*e.g.* the cartesian x, y, and z coordinates— and spins of all the system particles; for instance, of all electrons for the electronic Hamiltonian. This becomes a 4*N* coordinates problem, where *N* is the number of electrons. However, for DFT only one needs three, plus the spin.[16] Thanks to this, the computational costs are drastically reduced, particularly for medium and large systems with dozens to hundreds of atoms. In addition, while HF method does not take into account the correlation effects, DFT does.

Going into more detail, the functional of $\rho(r)$ can be separated (Eq. 6) into a part that includes the interaction between the external potential, $V_{ext}(r)$, and the electron density, and another part corresponding to a universal functional $F[\rho]$, which does not depend on the external position, *i.e.* the nuclei positions. There $V_{ee}[\rho]$ and $T[\rho]$ are included (Eq. 7), which are the coulomb repulsion between electrons, and the kinetic energy of electrons, respectively.

$$E[\rho(r)] = \int \rho(r) V_{ext}(r) dr + F[\rho(r)] \quad (6),$$

$$F[\rho(r)] = T[\rho] + V_{ee}[\rho] \quad (7).$$

In short, the Hohenberg and Kohn theorems ensure that the total energy of a many electrons system ground state is directly related with the electron density through a functional, but, however, there is no recipe to obtain the universal functional. Therefore, approximations are required for a correct practical DFT operation, where the Kohn Sham (KS) equations were presented.

In the KS method, one uses an imaginary system of independent electrons which do not interact with each other, with the same electron density of the studied system.[19] Equations 8 and 9 describe the KS hypotheses.

$$[\frac{-\hbar^2}{2m}\nabla^2 + V_s[\rho_0](r)]\varphi_i(r) = \varepsilon_i\varphi_i(r) \quad (8),$$

$$\rho_0(r) = \sum_i^N |\varphi_i(r)|^2 \quad (9).$$

There one finds first an expression for the electrons kinetic energy, and later the KS potential; the value of the effective local potential V_s determining the electron density, where ε_i represent the energies of Kohn-Sham orbitals, $\varphi_i(r)$, and by correspondence to the electronic density of the *N* particles that form the system. The main function of this approximation is to propose a form that allows the calculation of the total energy, although some terms of the equations do not have physical sense. For instance, the KS orbitals are indeed a mathematical construct, although in practice the look quite similar to the real orbitals.

These equations lack important terms from the interactions of electrons with each other: In particular, changes on the kinetic energy, and on exchange and correlation energies. All of them are described in the following energy exchange-correlation equation (Eq. 10), that depends on the electron density.

$$E = T_S[\rho(r)] + E_{ext}[\rho(r)] + J[\rho(r)] + E_{xc}[\rho(r)] \quad (10),$$

where one can find T_S, which is the kinetic energy of the fictitious electrons system; E_{ext} is the attraction between the electron density and the external potential; the term J contains the energetic repulsion between the electrons, and finally E_{xc} includes the exchange and correlation energies and the difference between the kinetic energy of the non-interacting system and the real one.[20]

The exchange-correlation energy, E_{xc}, can be calculated using an equation that contains quantum effects that have not been previously included.

$$E_{xc}[\rho(r)] = T_k[\rho(r)] - T_S[\rho(r)] + V_{ee}[\rho(r)] - J[\rho(r)] \quad (11),$$

where T_k and V_{ee} are properties of the real system, specifically, the kinetic energy and the repulsion energy. These two terms are not analytically known, and one needs ways to approach these terms. Unfortunately, this makes DFT an approximated method, even though it could be exact if such $E_{xc}[\rho(r)]$ was known.

5.1.3. Exchange-correlation energy

As above introduced, one of the main challenges for DFT is the search for an accurate exchange-correlation functional. The simplest approximation to calculate the E_{xc} it is the local density approximation (LDA), which assumes that the electron density does not vary much with

position, and therefore can be compared with an ideal electron gas system, named Jellium, of which we can know the correlation and exchange functionals. A derivation of this method is the local spin density approximation (LSDA), where the different components of spin, α and β, are taken into account, giving rise to two different electron density functions.[21]

In addition, there are more modern approximations for E_{xc}, such as the generalized gradient approximation (GGA), where the functional is a function of the electron density and its gradient. There are many different GGA functionals, and among them we could highlight the Perdew-Burke-Ernzerhof desnity functional (PBE),[22] which is the one used in the present work and suited for the energetic description of MXenes,[23] although other functionals could be appropriate, like PBE adapted for solids (PBEsol),[24] or the derived Viñes-Vega (VV) and VV for solids (VVsol) functionals.[23] Further than this, meta-GGA exchange-correlation functionals include the density, gradient, and second derivative to the mathematical expression, while hybrid functionals include a portion of HF exact exchange to the equation. Normally meta-GGA and hybrid functionals represent an improvement over GGA for molecules from main group elements, although for metallic systems, like the here-studied MXenes, GGA functionals are preferred.[23] In case one needs to consider the dispersive forces, not included by scratch in DFT, one could use any of the corrections developed in the last decades, including van der Waals (vdW) functionals, or even Tkatchenko-Scheffler or Grimme corrections. Here, the popular and extended D3 correction is used, as gives a balanced quantification of dispersive forces of systems adsorbed on metallic substrates, although other corrections would be probably adequate.[25]

5.2. COMPUTATIONAL MODELS

Apart from knowing how computational optimizations are to be carried out, one still needs to address the atomic models which would represent the real MXene systems. At this point, the arrangement of the atoms in a crystalline system is an important aspect when it comes to saving computational costs. We can differentiate two large groups of models for the representations of the solids: the cluster model and the periodic one. The choice of one model or another will depend on different aspects, and the computational power one disposes.[26] For instance, the cluster model is ideal for small clusters, but it is not the best representation for a large, macroscopic material, where it cuts a piece of the material; although can be adequate to study local properties. Another advantage is that allows for applying all possible methods of Quantum

Chemistry in an affordable way. However, for extended systems, the most used models are the periodic models, explained next.

5.2.1. Periodic model

The periodic model, used for this project, exploits the periodicity of a crystalline structure by imposing the infinite repetition of a unit cell in the three directions of space, simplifying the study of solids, *i.e.* a small unit cell with few atoms is enough to represent an infinite material. Bloch's theorem,[27] based on the periodicity of structures, described that the electronic motion in a solid and the shape of all wave functions must adjust to the periodicity. Within it, the orbital wavefunctions contain a periodic part, easily described by a plane wave. However, as a consequence of the periodicity imposing, the wavefunctions are defined by a vector located in the reciprocal space. Thus, for ordered crystals, the representation in the reciprocal space is more suitable, although the real space and the reciprocal are related in an indirectly proportional way; *i.e.* an increase in the distance in the real space leads to a decrease in the distance in the reciprocal space and *vice versa*.[28]

Thanks to the fact that this symmetry is always repeated in the three directions of space, the computational cost is significantly reduced, since only the atoms present in the unit cell are considered. In the case of MXenes, using this method is reasonable due to the 2D nature of these materials, in addition, to prevent interactions in MXenes layers, a vacuum of 10 Å is added between layers, as shown in Figure 2.

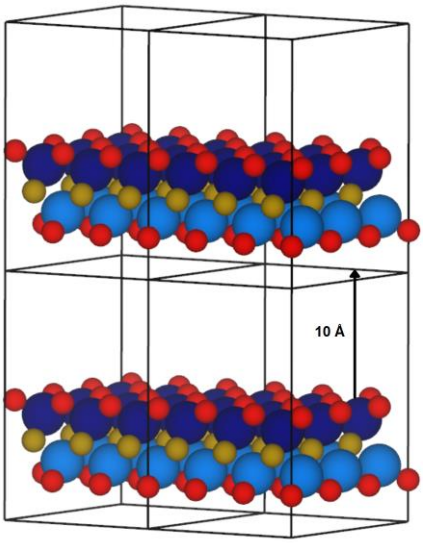

Figure 2. Representation on replicated unit cell of M_2CO_2 MXene including a 10 Å vacuum. Top and bottom metal atoms are shown by dark and light blue spheres, while C and O atoms are represented by brown and red spheres, respectively.

5.3. MXENES

The first 2D carbide MXene was discovered in 2011,[29] the Ti_3C_2, although a name was given for the family of materials, collectively called MXenes, in analogy to the graphene. These 2D materials have uncommon physical properties, most deriving from their TM carbide or nitride nature, implying good electrical and thermal conductivities, high melting points, and resistance, arising from their bonds, having contributions from metal, covalent, and ionic bondings.[30,31] The general formula of MXenes is $M_{n+1}X_nT_x$ (n = 1-3), where M is represented by an early TM, X represents C —in the case of our study— or N, and T_x are the surface terminations, in the present project T_x = O. MXenes are obtained by selective etching from a large family of compounds known as MAX phases,[32] where A is a *p*-block element, and are basically ternary carbides and nitrides; for instance, an example is Ti_3AlC_2, where Ti_3C_2 is isolated from removing Al using *e.g.* HF. So far, more than 20 MXenes have been isolated, and their number is growing.[29]

The precursor MAX phases display a $P6_3/mmc$ symmetry, where the TMs are packed in close-packed layers, while X atoms occupy octahedral voids. Thus, the resulting $M_{n+1}X_n$ phase

displays an ABC type of stacking. These $M_{n+1}X_n$ layers are glued together by close-packed *A* layers where the *M-A* bond is purely metallic, while *M-X* bonds have the aforementioned mixed character, and a stronger interaction. Taking advantage of the bond strength between *M-A* and *M-X*, the *A* layers can be chemically etched without breaking *M-X*, which comes handy to get the MXenes layers. To do so, a standard procedure implies that MAX phases are heated under vacuum at high temperatures using HF as an etching agent, although other F-free synthesis methods exist.[32] After etching *A*, the resulting powder is centrifuged for the correct separation of the solid and washed with deionized water until reaching values of pH between 4 and 6, and later sonicated and dehydrated. At this time, the structure of the material is similar to exfoliated graphite.[32] For the present study, we assume we have O-terminated M_2C MXenes, with general formula M_2CO_2, see Figure 3.

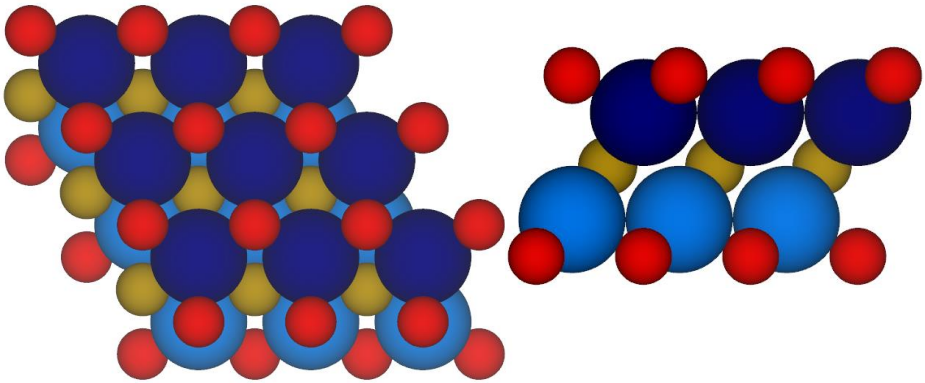

Figure 3. Different representations of a M_2CO_2 MXene *p*(3×3) supercell, from top (left) and side (right) views. Notice the preserved ABC stacking. Colour coding as in Figure 2.

Note in passing by that the MXene properties are affected by the T_x terminations. For instance, it has been shown that those that do not have any surface functionalization have a stronger metallic character, while other MXenes such as Sc, Ti, Zr, or Hf with the M_2CO_2 stoichiometry are semiconductors, or some Cr-based MXenes with F or OH terminations such as Cr_2CF_2, $Cr_2C(OH)_2$, or Cr_2NF_2 are ferromagnetic.[33] Clearly, such materials can be tuned so as to have profitable properties for energy storage applications, photo-, thermo-, and electro-catalysis, or their use as biosensors and gases sensors, among others.[33]

5.3.1. Single atom positions

In this study, nine different C-based MXenes (M_2CO_2) were studied (M = W, Ta, Hf, Mo, Nb, Zr, Cr, V, and Ti) with M being from Groups IV, V, and VI of the Periodic Table, see Figure 1. As single atoms, all 4*d* and 5*d* TMs will be sampled, since 3*d* TMs were already tested.[34]

For all the TM adatoms, four different high-symmetry positions were tested, including: Top, where the metal adatom is place directly on top of a surface O atom, HollowC, where the metal atom is placed on a three-fold hollow created by three surface O atoms, and laying on top of a subsurface C atoms, HollowM, similar to HollowC, but with a subsurface MXene metal atom directly underneath, and Bridge, where the metal adatom is placed bridging two vicinal surface O atoms, see Figure 4.

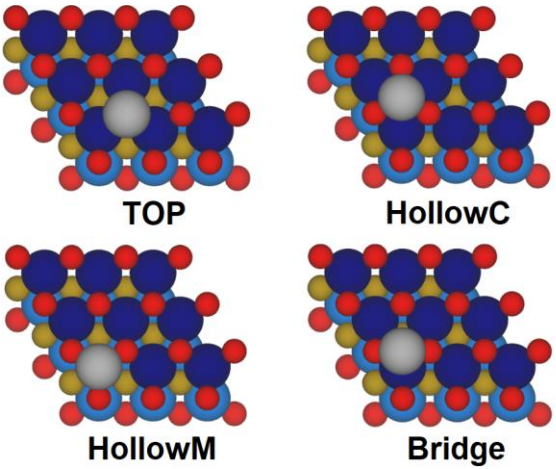

Figure 4. Top views of the tested sites placed in Top, HollowC, HollowM, and Bridge, respectively. Colour code as in Figure 2, while TM adatoms as shown as grey spheres.

5.4. Single Atom Energy Assessment

5.4.1. Adsorption energy

For each combination of 4*d* or 5*d* TM adatom and the MXene substrate, the interaction strength will be seized through the adsorption energy, E_{ads}, using the following equation:

$$E_{ads} = -[E_{TM/MXene} - (E_{MXene} + E_{TM})] \quad (11),$$

where $E_{TM/MXene}$ is the energy of the M_2CO_2 MXene with the TM adatom optimized upon, E_{MXene} is the energy of the M_2CO_2 MXene, and E_{TM} is the energy of the isolated TM atom.[35] The formula is defined in such a way that E_{ads} is positive for a more accurate graphic display, since the higher the adsorption energy, the greater the bond between the atom and the MXene. As above stated, when carrying out the calculations, one has to take into account that the dispersive forces must be included, even if their role is minor for strong bonds governed by the electronic part,[22] and we will do that using Grimme D3 correction (PBE-D3).[36] Generally, E_{ads} values in between 0 and 0.3 eV could be attributed entirely to dispersive forces, while larger ones will have increasingly important electronic contributions.

5.4.2. Cohesive Energy

The cohesive energy, E_{coh}, of the explored TM bulks is an important feature when describing the single atom energetic stability. E_{coh} is defined as the energy necessary to separate the condensed bulk material into free, isolated atoms, and so the higher the E_{coh}, the greater the bonds in the bulk, and the stability of the crystalline structure.[37]

For the present study, this parameter will be used to know whether there is a thermodynamic preference of the single adatoms to gather and form clusters, or, on the contrary, to be isolated. This can be assessed by the following equation:

$$E_{diff} = E_{ads} - E_{coh} \quad (12),$$

where a negative E_{diff} implies that the bond of the single adatom on the MXene is smaller than the bonds created in the TM bulk structure, and so, the latter situation is more stable. Thus, the single adatoms would be energetically driven to form clusters. However, when E_{diff} is positive, the situation is the other way around; the bond of the single adatom to the MXene is stronger than in the bulk, and so energetically preferred. This indeed implies that supported clusters or nanoparticles would be energetically driven to disperse over the materials, if possible, although, of course, one would need to regard kinetic and coverage effects. The cohesive energies used here are taken from literature and calculated in the same computational way as the current optimizations, so are usable with no risk of adding systematic errors arising from different computational setups.[38]

6. COMPUTATIONAL DETAILS

Within this work, the DFT calculations were carried out spin-polarized, and so, allowing for having unpaired electrons. All the optimizations were performed using *Vienna ab initio simulation package* (VASP) suite.[40] All DFT optimizations were carried out using the Perdew-Burke-Ernzerhof (PBE) exchange-correlation functional,[22] and, when required, adding Grimme D3 correction for the treatment of dispersive forces (PBE-D3).[36] Core electrons were described using projector augmented wave (PAW) pseudopotentials,[41] while valence electrons density was expanded on a plane-wave basis set with a 415 eV kinetic energy cutoff, enough to provide converged and reliable adsorption energy estimates on MXenes.[41] Optimizations stopped when forces acting on nuclei were below 0.01 eV· $Å^{-1}$, while the electronic energy was converged under 10^{-6} eV. In order to speed up the convergence, a tetrahedron smearing of 0.2 eV width was used, although final total energies were extrapolated to 0 K. All atoms were fully allowed to relax during optimizations, although restrictions were applied when exploring diffusive paths, see below.

To model low-coverage adatom situations, *p*(3×3) supercell M_2CO_2 models were used. In order to avoid interactions between MXenes, the height of the supercell was set to 16 Å, so that a minimum of 10 Å vacuum space is placed between MXene sheets repeated perpendicular to surface planes. In order to sample electronic bands within the reciprocal space, we used a Monkhorst-Pack grid[42] of 5×5×1 special **k**-points. For the optimization of single TM atoms in the vacuum, an asymmetric cell of 9×10×11 Å dimensions was used, carrying out calculations at Γ-point, and ensuring the correct, expected orbital occupancy and electronic configuration. Almost 750 optimizations were carried out in this project, and we are thankful to the *Red Española de Supercomputación* (RES) for the project QHS-2021-3-0006 and access to Calendula/Scayle supercomputer, without which such a high-throughput study could have not been possible.

7. RESULTS AND DISCUSSION

In this section we will discuss the results obtained from the interaction of the studied TM adatoms belonging to *4d* (Y, Zr, Nb, Mo, Tc, Ru, Rh, Pd, Ag, Cd) and *5d* (La, Hf, Ta, W, Re, Os, Ir, Pt, Au, Hg) TM series, with MXenes substrates with M_2CO_2 formula (M= Ti, Zr, Hf, V, Nb, Ta, Cr, Mo, W), belonging to TMs from group IV (M = Ti, Zr, Hf), V (M = V, Nb, Ta), and VI (M = Cr, Mo, W). These hybrid compounds are labelled hereafter as TM@MXene.

7.1. TM@MXENES: SITE AND STABILITY

As aforementioned, different adsorption sites were considered, all with high-symmetry, see Figure 4, labelled as Top (T), HollowC (H_C), HollowM (H_M), and Bridge (B). After analysing the interaction mapping of the studied TMs on the selected MXenes, one can conclude that the H_C site is the most stable site for the majority of 4*d* TMs. However, there are few exceptions to this statement, as Ag@Hf_2CO_2 prefers T sites, and Ag@Cr_2CO_2 B sites. On the other hand, Cd single atoms prefer the H_M on Hf_2CO_2, Cr_2CO_2, Ta_2CO_2; whereas the B site is the most suitable on V_2CO_2 and Nb_2CO_2. Furthermore, the B site is more stable for Rh and Pd atoms over V_2CO_2 and Mo_2CO_2, respectively. Finally, the H_M is favourable for Pd over W_2CO_2. From the above, the H_C site preference is general, but particular deviations are found for weakly interacting TM adatoms (see below), and for the Cr_2CO_2 MXene substrate. The particular E_{ads} values are discussed next.

7.2. TM@MXENES: ADSORPTION ENERGIES

To clarify the trends of the TMs anchored on MXene surfaces, we firstly focus on the 4*d* TM adatoms, and later on the 5*d* ones. Note that the E_{ads} is initially calculated for all four possible sites at PBE level, and only the most stable site is recalculated using Grimme's D3 correction. The later set of calculations are selected to get the main conclusion of this study. Note in passing by that test calculations on selected systems at PBE-D3 level on all sampled sites systematically delivered that PBE most stable site is indeed the one achieved at PBE-D3 level.

7.2.1. Adsorption energies of 4*d* TM adatoms

The adsorption energy of 4*d* TM adatoms over MXenes, calculated as defined in Eq. 11, are listed in Table 1. The largest TM@M_2CO_2 interactions occur with W_2CO_2, where in some cases they exceed the 10 eV (*e.g.* Y, Zr, and Nb adatoms), whereas the smallest interactions are found for the Hf_2CO_2 MXene. In all cases, Ag and Cd TMs, especially Cd, have a much smaller E_{ads} compared to other TM adatoms; in many cases approaching the physisorption limit of 0.3 eV. This is explained based on their stability and d^{10} electronic configuration, which makes them much less chemically active in comparison.

MXene\TM	Y	Zr	Nb	Mo	Tc	Ru	Rh	Pd	Ag	Cd
Ti_2CO_2	6.89	7.53	6.36	4.34	4.13	4.12	3.76	2.74	1.55	0.72
Zr_2CO_2	5.56	5.89	4.93	3.33	3.10	3.29	2.75	1.76	0.93	0.34
Hf_2CO_2	4.04	4.42	4.92	2.31	2.34	2.92	2.46	1.58	0.47	0.30
V_2CO_2	8.23	9.34	8.87	6.91	6.46	5.81	5.13	3.58	2.69	0.38
Nb_2CO_2	6.87	7.23	5.65	3.63	3.44	3.47	2.92	1.92	1.35	0.56
Ta_2CO_2	5.28	5.56	4.56	2.67	3.26	3.20	3.12	1.96	1.05	0.38
Cr_2CO_2	8.58	11.57	10.87	9.40	6.92	6.84	6.10	5.11	2.93	0.48
Mo_2CO_2	10.37	11.20	10.04	7.99	7.41	7.38	6.04	4.69	4.19	3.09
W_2CO_2	10.05	11.18	10.34	7.84	8.38	8.41	7.58	5.80	4.97	4.09

Table 1. E_{ads} of 4*d* TM adatoms over M_2CO_2 systems as gained by PBE-D3 calculations.

To visualize this data, and to capture trends, Figure 5 shows the E_{ads} variation along the 4*d* series. The general, overall trend, regardless of the M_2CO_2 substrate, is that E_{ads} decreases when moving right on the Periodic Table; this is, decreases as the number of TM adatom *d* electrons increases. The fine detail reveals, though, that the adsorption energy shows a two-hump shape, featuring minima in the trend near Mo or Tc atoms, this is, when reaching a d^5 electronic configuration. This, together with a minimum for Ag and Cd d^{10} type of electronic configuration reinforces previous observations showing that E_{ads} is affected by the isolated TM adatom stability, and so, half-full and full *d*-band occupations, being more stable, feature smaller E_{ads} values, a point observed earlier on other 2D materials, such as graphene and graphyne.[7,8] Aside, one observes as well how the substrate influence the single atom bonding, with changes in between the lowest binding Hf_2CO_2 MXene, and the strongest binding MXene, W_2CO_2, which

reach nearly 6 eV across the 4*d* series. Along this line, it seems that TM adatom adsorption strength decreases when going down a MXene group, *e.g.* down Group IV M_2CO_2 (Ti, Zr, Hf), so that E_{ads} of Ti_2CO_2 > Zr_2CO_2 > Hf_2CO_2. The same trend is observed for Group V MXenes, although for Group VI, the trend is broken, as, in general, W_2CO_2 > Mo_2CO_2 > Cr_2CO_2, although crossovers are found along the 4*d* series. For instance, the bonding is strongest on Cr_2CO_2 for Zr, Nb, and Mo, *i.e.* for early TM adatoms; although that is not the case for Y. Moreover, it seems as the TM E_{ads} strengthens as going right the groups of M_2CO_2 substrates; this is, is stronger for Group VI cases (Cr_2CO_2, Mo_2CO_2, and W_2CO_2), and weakest for Group IV cases (Ti_2CO_2, Zr_2CO_2, and Hf_2CO_2).

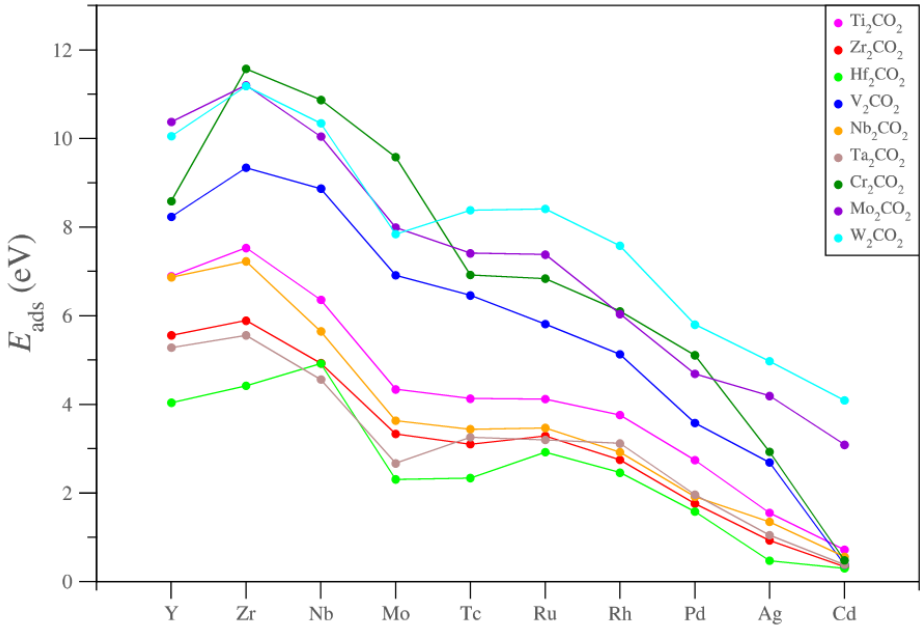

Figure 5. Evolution of E_{ads} for the 4*d* series TMs on different M_2CO_2 surfaces.

7.2.2. Heights of TM adatoms with respect M_2CO_2 for the 4*d* series

Having discussed the E_{ads} values in the last section for the 4*d* TM adatoms, we inspect further the adatom distance with respect to the MXene surface, labelled as *h*. To do so, the surface O mean height is calculated, and the adatom height measured with respect the mean O height. This structural analysis would be interesting, since one could find out a plausible relationship

between the height and the E_{ads}; for instance, one would expect smaller *h* values for large E_{ads} values, and *vice versa*.

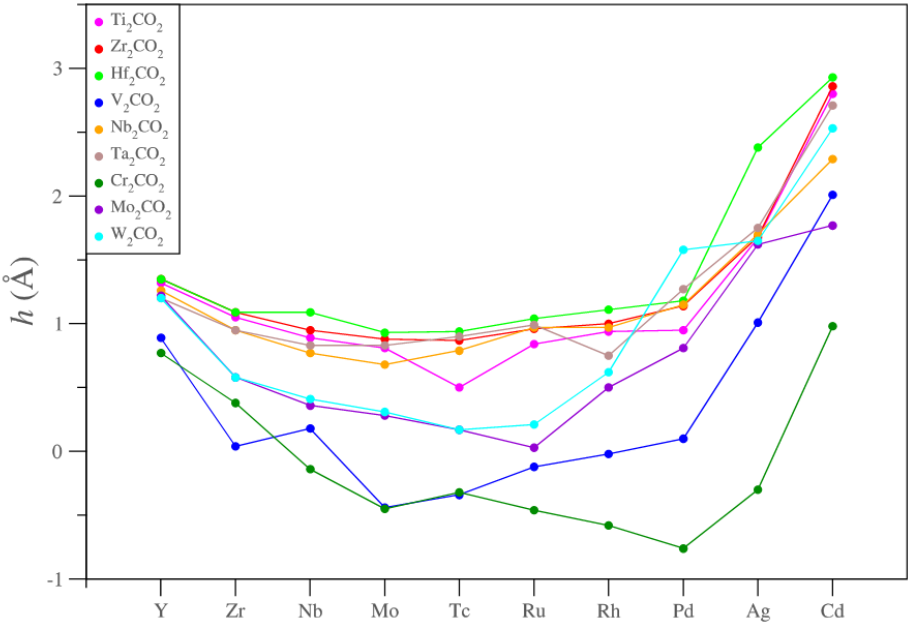

Figure 6. Evolution of *h* along the 4*d* series for all TMs adsorbed on the different M_2CO_2.

As one can see in Figure 6, there is a correspondence with some of the energetic aspects. For instance, the strongest E_{ads} for Group IV M_2CO_2 is translated into smaller heights, to the point of the absorption for many cases of Cr_2CO_2 and V_2CO_2. Furthermore, d^{10} Ag and Cd show a noticeable increase of the *h* values, a point that, together with the relatively small E_{ads}, goes for a physisorption situation. Further than this, *h* is linearly correlated with respect E_{ads} for the nine different studied MXenes in Figure 7. In all cases a trend is captured, as expected, showing that, the larger the E_{ads}, the smaller the *h*. However, the linearity of this relation is far from desirable, as the regression coefficients, R, are quite small, being the largest for Ta_2CO_2, of 0.69, and so, the height is not only governed by the adsorption strength yet influenced by it.

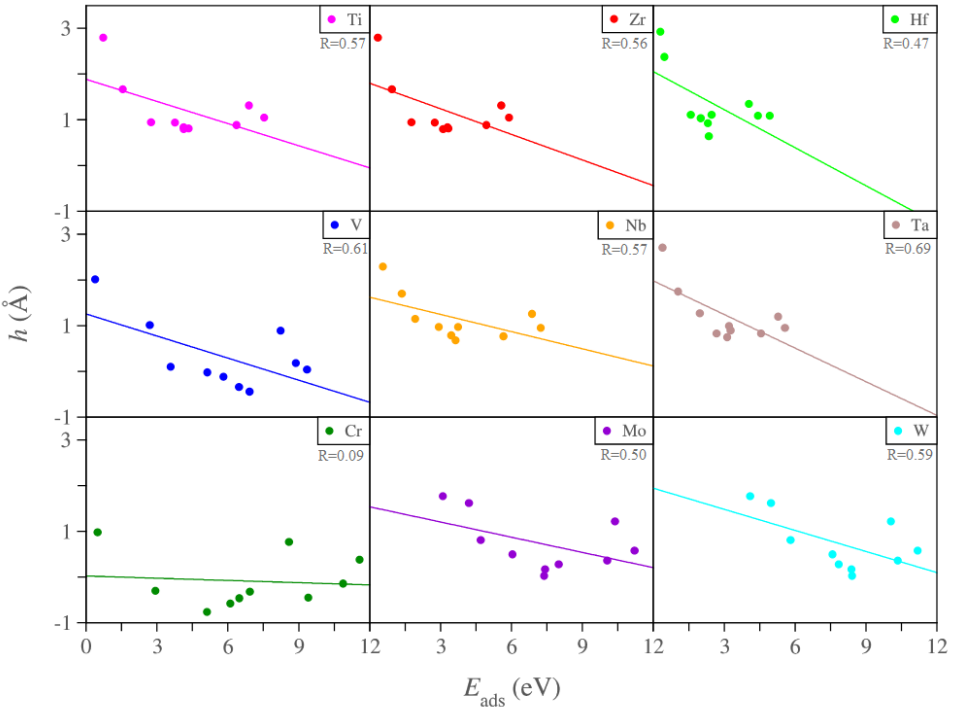

Figure 7. Linear correlation of *h* values with respect E_{ads} for the 4*d* TM adatoms on the nine explored M_2CO_2 MXenes.

It is worth mentioning that, for two MXenes (Cr_2CO_2 and V_2CO_2), some of the h values are negative; particularly for middle TMs. In these situations, the TM adatom penetrates the surface O-layer, placing itself in between the MXene M (Cr or V) and the O layer, see a representative case in Figure 8 for Nb on V_2CO_2. Still, such atoms are not fully hidden, and could be reached by reactant species being present on the material surface.

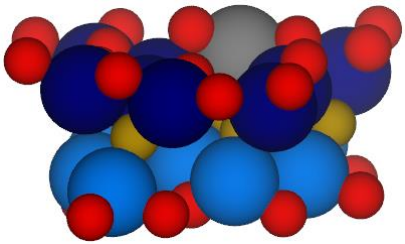

Figure 8. Side view of Nb in V_2CO_2, color coding as in Figure 4.

7.2.3. Isolating or clustering trends for 4*d* TM adatoms

To test whether, thermodynamically, the TM adatoms would tend to form clusters or, on the contrary, to be isolated, we use Eq. 12 to compare adsorption energies with respect TM bulk cohesive energies, calculated previously in the literature using the same computational setup as here used.[37] According to Eq. 12, single atoms isolation would be energetically favorable for positive values of E_{diff}, *i.e.* $E_{diff} > 0$, whereas atomic clustering would be favorable for $E_{diff} < 0$. One must keep in mind that, in some cases, where E_{diff} is close to 0.2 eV, and due to the intrinsic error of the DFT method, which is *ca.* of the same order, one could consider SA isolation and TM clustering competitive for the $E_{diff} \pm 0.2$ eV range. These cases are rare, and only few are highlighted, and listed in Table 2. For such cases, the preferential for isolating or clustering is not clear, and would require extra calculations, *e.g.* using different exchange-correlation functionals, or other wavefunction methods of better accuracy.

TM	MXene	E_{diff} [eV]
Tc	Mo_2CO_2	0.02
Ru	Mo_2CO_2	0.18
Rh	Mo_2CO_2	-0.06
Ag	W_2CO_2	0.06

Table 2. E_{diff} values close to zero, where it is difficult to forecast isolated atoms or clustering preference due to DFT inaccuracy.

Apart from these cases, which have been identified, the rest are clearly going for isolating atoms situations or atomic clusters, as shown in Figure 9. As one can easily observe, there is a concave shape trend, explained again due to the TM electronic configuration and *d*-band filling. Those TM adatoms with few number of *d* electrons imply that they are filling bonding states of the *d*-band, but, since their number if small, the bond strength in the bulk, *i.e.* the bulk cohesive energy, is small. This results in cases where it is easy to get TM adsorption energies larger than E_{coh}, and so, easy to get positive E_{diff} values. In the other extreme, situations near or at a d^{10} configuration implies that half of electrons occupy bonding states, but this positive effect on the E_{coh} is counteracted by the other half of the electrons occupying antibonding states, which eventually translate in small E_{coh} values, and so, situations where E_{ads} are easily larger than

E_{coh}, and so, positive values of E_{diff}. Finally, those situations with a near d^5 electronic configuration imply *d* electrons occupying bonding states in the bulk, maximizing the E_{coh}, and making positive E_{diff} values very difficult. That is why the valley minimum is found for d^5 Tc, with close exceptions like minimum being Ru for V_2CO_2 and Rh for Mo_2CO_2. Exceptions are found as well for extremes, like peaks being Zr instead of Y for Cr_2CO_2, or. Ag in V_2CO_2 instead of Cd. In any case, the general trend is well preserved.

Other than this, the trends towards positive E_{diff} follow the same trends towards large E_{ads} values as seen before. In this sense, Group IV MXenes (Cr_2CO_2, Mo_2CO_2, and W_2CO_2) tend to have single atoms, together with V_2CO_2, while for the rest, the overall trend would be to have TM clustering. Such MXenes are highlighted ideal supports for SACs in general, with the particular aspect that they are able to isolate Pt-group Ru, Rh, Pd, and Ag metals.

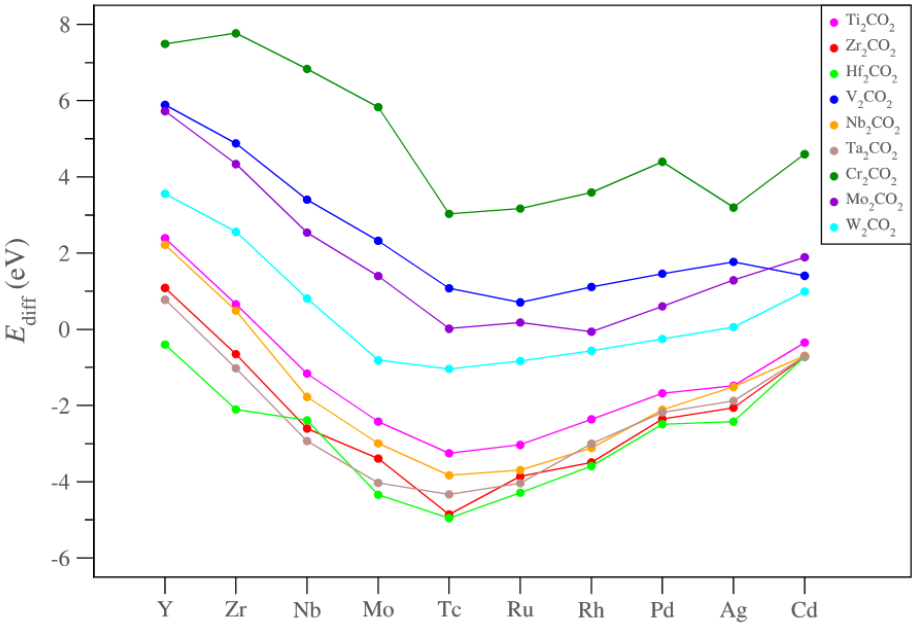

Figure 9. Evolution of E_{diff} along the 4*d* TM series for all M_2CO_2 substrates.

7.2.4. Adsorption energies of 5*d* TM adatoms

The same procedure carried out for 4*d* TM adatoms has been done now for 5*d* TM adatoms. The adsorption energies are shown in Table 3, and, again, one observes largest adsorption energies for Cr_2CO_2, followed closely by W_2CO_2 and Mo_2CO_2, all belonging to Group VI M_2CO_2 MXenes. As shown for 4*d* TMs, the atoms with the smallest E_{ads} are Au and Hg, with full d^{10} configuration, while strongest bonds are shown for earlier TMs. Following the 4*d* analysis, Figure 10 represents the E_{ads} variation of the 5*d* TM adatoms along the *d* series. As happened for 4*d* TM adatoms, there is a general, overall trend in that the E_{ads} decreases as the number of *d* electrons increases, reaching situations close to physisorption, *i.e.* with E_{ads} below 0.3 eV, for d^{10} cases such as Au and Hg, in an analogous fashion as happened with Ag and Cd 4*d* TM adatoms. Further than that, one still observes the two-hump shape —seagull for Group IV MXenes—, with a minimum centered for Re. Last but not least, some trends are repeated, *i.e.* E_{ads} getting weakened down a group, and strengthened along the MXene *d* series, with some exceptions found only for Group VI MXenes.

MXene\TM	La	Hf	Ta	W	Re	Os	Ir	Pt	Au	Hg
Ti_2CO_2	7.98	7.80	7.65	6.05	4.63	4.32	4.47	3.84	1.28	0.69
Zr_2CO_2	6.72	6.08	5.85	4.20	1.02	2.87	2.86	2.24	0.65	0.31
Hf_2CO_2	5.16	4.51	4.32	3.06	0.49	2.35	2.57	2.07	0.60	0.30
V_2CO_2	8.78	9.82	9.39	9.08	6.55	6.89	5.57	4.72	2.03	0.15
Nb_2CO_2	8.11	7.42	7.09	5.02	3.39	3.88	3.80	2.76	0.76	0.38
Ta_2CO_2	6.49	5.78	5.34	3.66	1.16	3.53	3.82	2.79	0.93	0.34
Cr_2CO_2	10.13	12.60	12.46	11.70	8.75	9.86	6.90	4.68	4.63	2.04
Mo_2CO_2	11.69	11.33	8.95	9.93	8.20	8.11	7.47	6.07	3.63	2.80
W_2CO_2	11.56	11.49	11.63	10.16	8.66	8.85	8.53	7.64	4.92	3.97

Table 3. E_{ads} of 5*d* TM adatoms over M_2CO_2 systems as gained by PBE-D3 calculations.

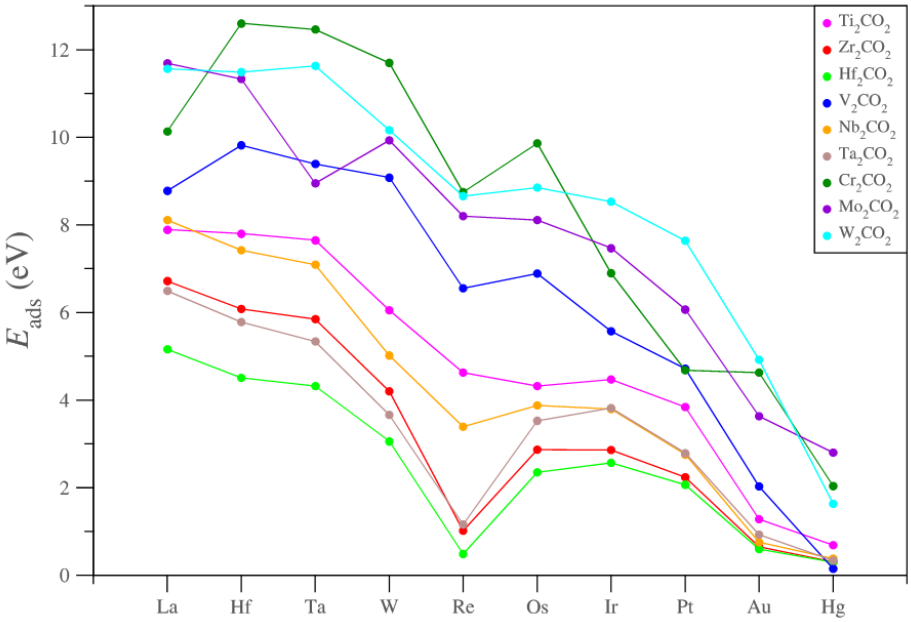

Figure 10. Evolution of E_{ads} for the 5*d* series TM adatoms on different M_2CO_2.

7.2.5. Heights of TM adatoms with respect M_2CO_2 for the 5*d* series

In this section we will try to identify again a plausible relationship of the adsorption energy with respect the height at which the TM adatoms sit. The results, shown in Figure 11, reveal again a trend towards having physisorption for Au and Hg atoms, although unusually large values are found for Pt on W_2CO_2, and also for d^5 Re on Zr_2CO_2, Hf_2CO_2, and Ta_2CO_2, which coincide with the seagull shape minima in Figure 9, belonging to very weakly adsorbed situations.

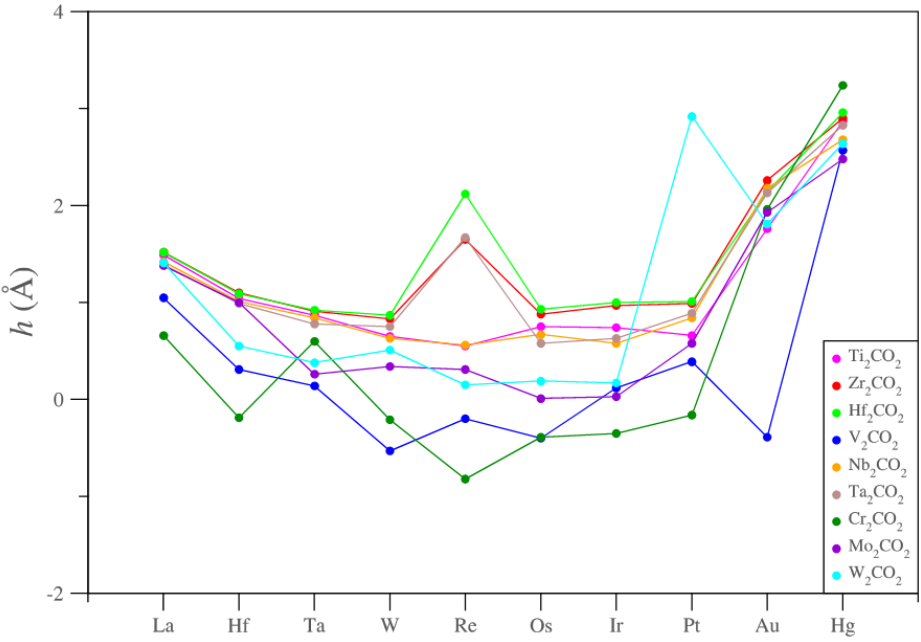

Figure 11. Evolution of *h* along the 5*d* series for all TM adatoms adsorbed on the different M_2CO_2.

To confirm the aforementioned relation in between E_{ads} and *h*, a plot is carried out similarly as done in Figure 7 for 4*d* TM adatoms, and shown here for 5*d* TM adatoms in Figure 12. In all cases the expected trend, this is, smaller *h* for larger E_{ads}, is systematically found; however, the trends cannot be called linear, as the highest regression coefficient is only of 0.73, found for Hf_2CO_2. Still, the results, in average, are better for 5*d* than for 4*d*, but this can be attributed to more disperse E_{ads} values, which help in the regression coefficient. In any case, the height is not only biased by the adsorption strength, but definitely is one of the factors affecting it. As happened as well for 4*d* TMs, there are few cases for Cr_2CO_2 and V_2CO_2 MXenes where the TMs feature negative h values, implying that the TM adatoms place in between the surface O layer and the MXene Cr or V layer.

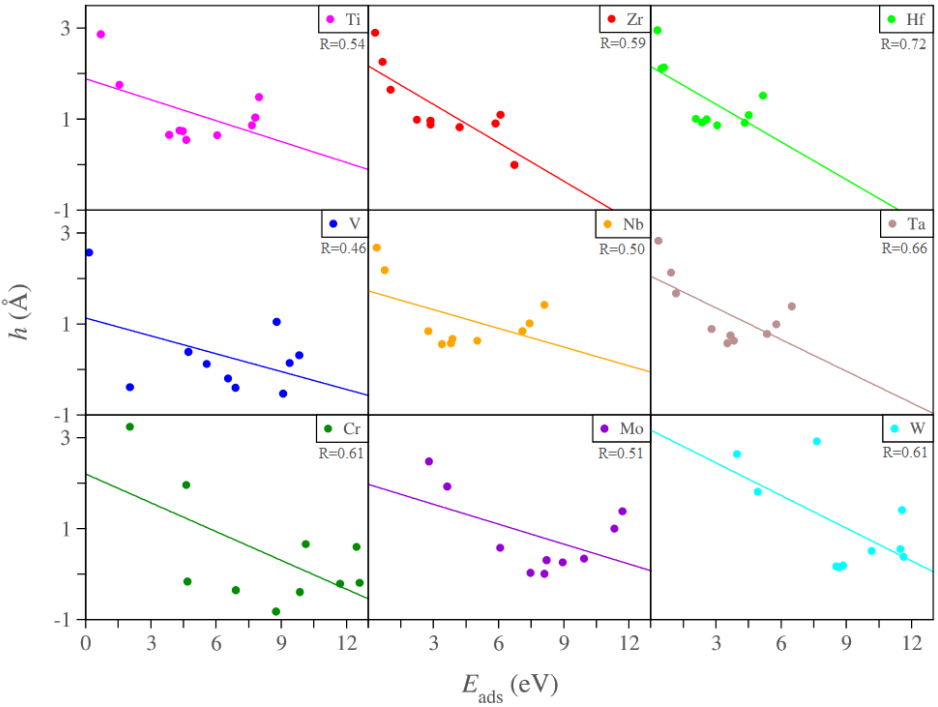

Figure 12. Linear correlation of *h* values with respect E_{ads} for the 5*d* TM adatoms on the nine explored M_2CO_2 MXenes.

7.2.6. Isolating or clustering trends for 5*d* TM adatoms

As done for 4*d* TM adatoms, here we evaluate the E_{diff} values, comparing TM adatoms E_{ads} *vs.* E_{coh} values.[38,39] Again, some cases are unclear within the DFT ± 0.2 eV accuracy, shown in Table 4.

TM	MXene	E_{diff} [eV]
Pt	Mo_2CO_2	-0.01
Au	Mo_2CO_2	0.20
Ir	W_2CO_2	-0.17
Hg	Zr_2CO_2	-0.13
Hg	Hf_2CO_2	-0.13

Hg	Nb_2CO_2	-0.14
Hg	Ta_2CO_2	0.14
Pt	W_2CO_2	-0.17

Table 4. E_{diff} values close to zero, where SA or clustering preference is unclear.

As happened with 4*d* TM adatoms, these limit cases imply generally Mo_2CO_2 and W_2CO_2 cases, and late TM adatoms. Moving forward, Figure 13 shows the E_{diff} values across the 5*d* series. The trend is similar to the 4*d* TM adatoms, in the sense that valley shapes are obtained, with maxima at earliest and latest TMs. However, for 5*d*, the minimum is observed for Pt atoms. Once more, Group VI MXenes (Cr_2CO_2, Mo_2CO_2, and W_2CO_2) plus V_2CO_2 are the best substrates to have isolated TM atoms. It is noticeable, though, how late TMs such as Re, Os, Ir, and Au can be isolated on some MXene cases, being posed as ideal materials for SACs.

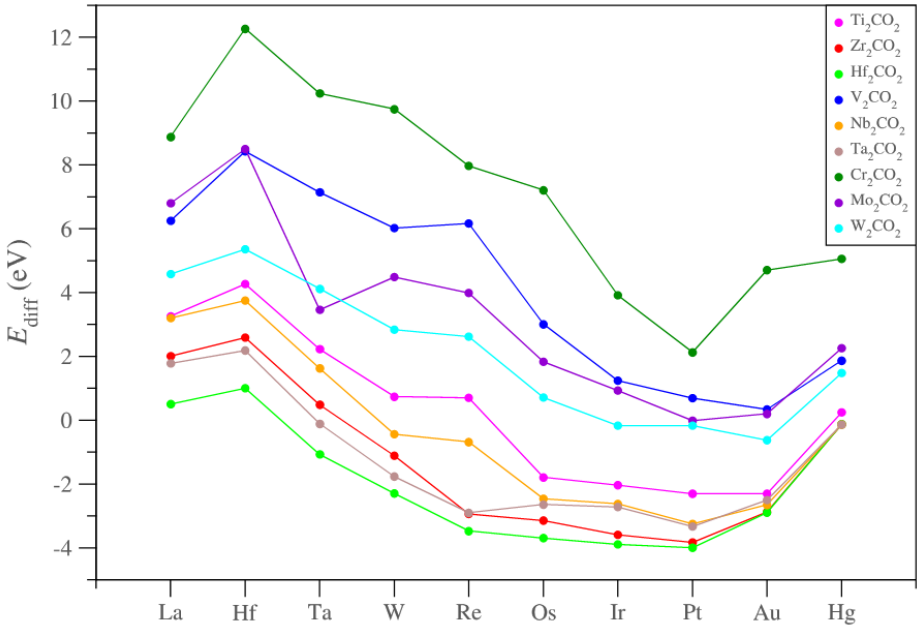

Figure 13. Evolution of E_{diff} along the 5*d* TM series for all M_2CO_2 substrates.

In short, similarly to 4*d* TM adatoms, one can state that the M_2CO_2 with M = Cr, Mo, W, and V have an energetic preference towards isolating 5*d* TM adatoms, while for the rest, there is a

trend towards TM clustering. Having analyzed 4*d* and 5*d* TM adatoms, a comparison between them, as well as on previous 3*d* TM adatoms, is explained next.

7.2.7. Different series comparison

Having analyzed 4*d* and 5*d* series by themselves, and having observed trends along groups and series for M_2CO_2 MXene substrates that favor the TM single-atom situation, it would be now interesting to make the comparison relating the *3d*, 4*d*, and 5*d* TM series to look for similarities or differences. The values of 3d are taken from the literature, gained using the same calculation setup, procedure, basis set, etc… so can be safely compared without bringing in any sort of systematic errors.[34]

Figure 14 shows the E_{diff} between the adatoms belonging to the same group and different *d* series on the nine studied M_2CO_2 MXenes. Generally, *3d* adatoms are the ones with the highest cohesive energies, and so are more prone to clustering, followed by 4*d* and 5*d*. Thus, E_{diff} are generally larger for 5*d*, and decrease in the sequence 5*d* > 4*d* > 3*d*, although the trends are not exempt of exceptions. For instance, the trend is well kept for early TMs, but for late TMs it appears as 4*d* are more prone to isolation than 5*d*, seen e.g. in Group X TMs (Ni, Pd, Pt), while 3*d* can be more prone to isolation than 4*d* for middle TM groups, like seen in some cases of Groups VI (Cr, Mo, W), VII (Mn, Tc, Re), and VIII (Fe, Ru, Os).

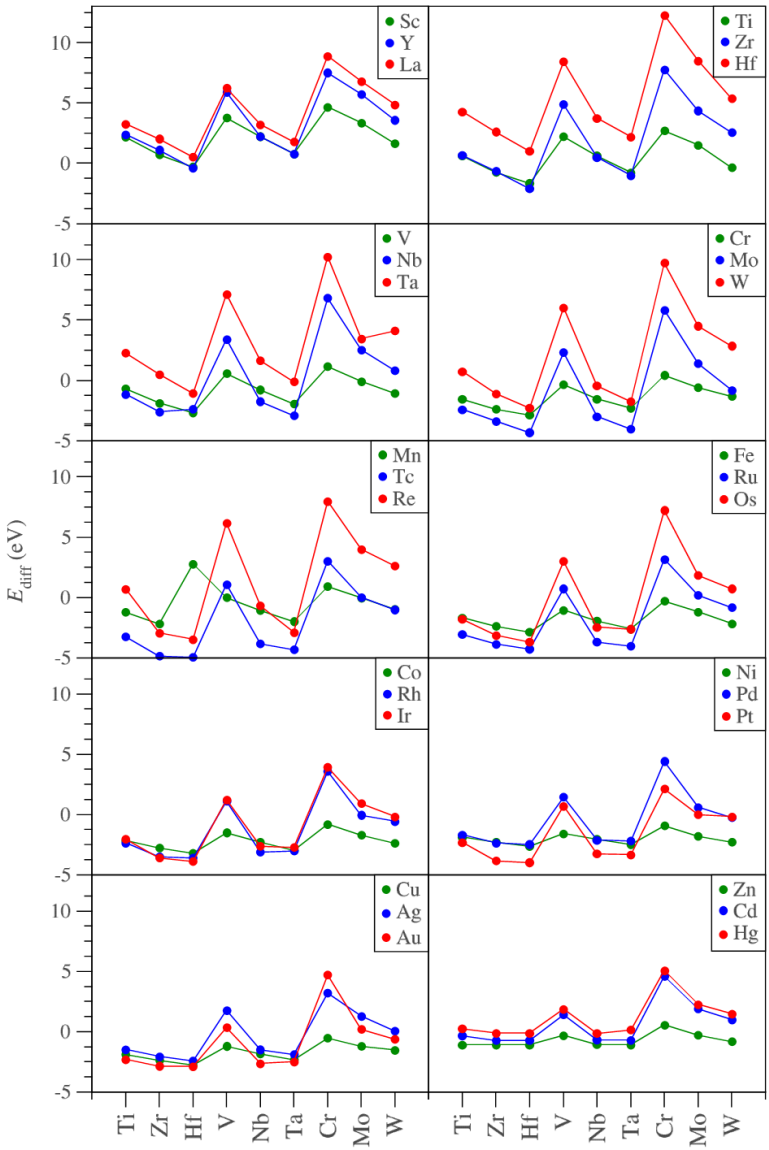

Figure 14. E_{diff} trends for 3*d*, 4*d*, and 5*d* TM adatoms on the studied MXenes.

7.3. DIFFUSION ASPECTS

Having analyzed the energetic stability in the previous sections, one may wonder whether kinetics could play a role. The answer is positive; for instance, some of the previous TM adatoms may display negative E_{diff} values, and, therefore, a tendency to cluster. But, if their diffusion on the MXene surface is inhibited, due to large diffusion energy barriers, their agglomeration would be kinetically inhibited, as the atoms would not meet each other. The other way around, for those cases with a positive E_{diff}, one would expect clusters or nanoparticles to disaggregate into isolated single-atoms; however, that would be prevented if diffusion would be energetically costly, this is, with large diffusion energy barriers. The exploration of diffusion energy barriers for each case is out of the limits for the present work, but we pretended to get some insights, at least for a couple of cases, related to low and high adsorption energies. To this end, we chose the same MXene substrate (Hf_2CO_2), and Ag and Mo adatoms, with E_{ads} of 0.47 and 2.41 eV, respectively. Figure 15 shows the explored diffusion energy paths for both cases.

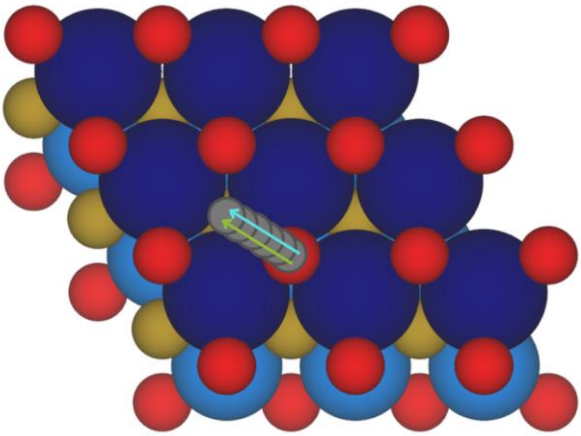

Figure 15. Diffusion pathways studied for Ag (blue) and Mo (green)

Along the paths, different intermediate situations were calculated, obtained by linear interpolation of positions in between found minima. To avoid these intermediate situations to fall into minima in the course of the DFT optimizations, the TM adatom was allowed to move only in the direction perpendicular to the surface, while the bottommost O layer of the MXene was kept fully frozen to avoid slab drifting, while the rest of degrees of freedom were fully allowed to relax. Figure 16 shows the Ag@Hf_2CO_2 case, where Ag adatom moves from T to H_C position. The

profile reveals, on point 6, another minimum, not previously found, a feature that is sometimes found for weakly adsorbed situations, *i.e.* physisorption, where the adsorption is not site-specific and many different minima can exist, and not necessarily on high-symmetry sites.[7] For this particular case, the diffusion energy is found to be minimal, here estimated to be *ca.* 0.003 eV, and so, basically negligible, point that would suggest that Ag atoms are highly mobile on Hf_2CO_2. Note that this is a preliminary evaluation, and one would require refining the obtained transition states, and characterize minima and transition states as so through a vibrational frequency analysis.

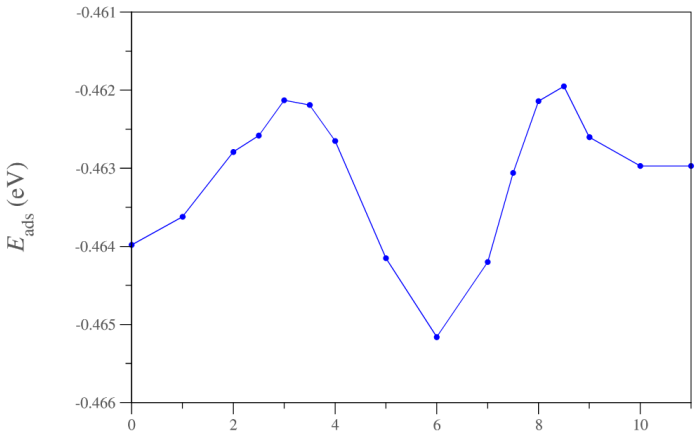

Figure 16. Ag@Hf_2CO_2 diffusion energy profile; negative E_{ads} are shown for commodity.

Figure 17 shows the energetic profile of Mo@Hf_2CO_2. One can see that the system is dominated by a single, profound minimum, and diffusion requires jumping out of it, to reach a plateau of energy. In this case, one departs from Top to H_C, and diffusion would require overcoming a barrier of 1.18 eV, which is significant. One could safely state that Mo is chemisorbed on Hf_2CO_2. Even if Figure 9 shows a negative E_{diff}, implying Mo atoms aggregation, this would be impeded by the SA diffusion, which would allow for a certain survival of Mo adatoms under working conditions. Thus, the SACs capabilities could be enlarged by considering kinetics.

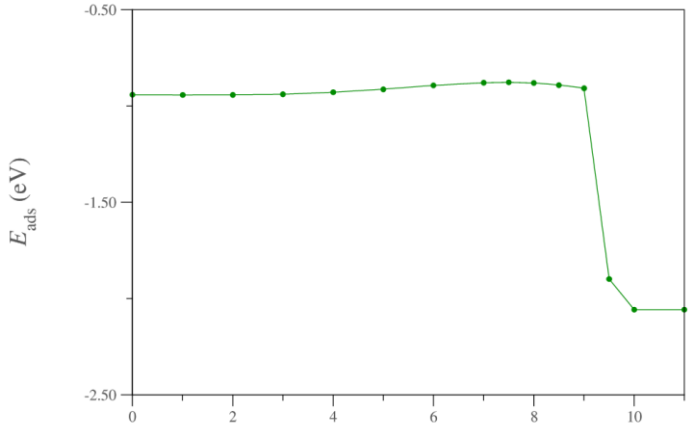

Figure 17. Mo@Hf_2CO_2 diffusion energy profile; negative E_{ads} are shown for commodity.

8. CONCLUSIONS

Once all the necessary calculations have been carried out, and the data analyzed, the following specific conclusions can be withdrawn, in accordance to the outlined study objectives. In particular:

- Generally, the most stable site for 4*d* and 5*d* TM adatoms on M_2CO_2 MXenes is H_C, although some exceptions are found, particular for late TM adatoms, featuring Top, Bridge, or H_M sites.
- The adsorption energies can be very high, particularly for early TM adatoms, and the E_{ads} values decay along the *d* series, reaching basically physisorption situations for TM adatoms with d^{10} electronic configuration.
- Lowest E_{ads} are found for particularly stable TM adatoms, those with d^5 and d^{10} electronic configuration.
- The TM adatom height is influenced by the E_{ads}; the larger the E_{ads}, the smaller the *h*.
- The TM E_{ads} is stronger when going along the *d* series for M_2CO_2 MXenes, and weakened down a group.
- The atomic isolation, seized by E_{diff} values, show a preferential SAC situations for early and late TM adatoms, and particularly enhanced on V_2CO_2, Cr_2CO_2, Mo_2CO_2, and W_2CO_2 MXenes.
- Kinetic aspects may play an important role in determining whether SACs can be kinetically stable or not, as shown on Mo on Hf_2CO_2.

9. REFERENCES

1. Jun, L.; Stephanopoulos M.; Xia, Y. Introduction: Heterogeneous Single-Atom Catalysis. *Chem. Rev*. **2020**, *120*, 11699-11702.
2. Morales-García, Á.; Calle-Vallejo, F.; Illas, F. MXenes: New Horizons in Catalysis. *ACS Catal*. **2020**, *10*, 13487-13503.
3. Morales-García, Á.; Viñes, F.; Gomes, J.R.B.; Illas, F. Concepts, Models, and Methods in Computational Heterogeneous Catalysis Illustrated through CO_2 Conversion. *Wiley Interdiscip. Rev. Comput. Mol. Sci*. **2021**, 11, e1530.
4. He, H.; Hudson, W.; Junjian, L.; Xujun, L.; Wizum, L.; Yannan, W. Research Progress and Application of Single-Atom Catalysts: A Review. *Molecules.* **2021**, *26*, 650.
5. Martínez, B.; Viñes, F.; McBreen, P.T.; Illas, F. Mo Single Atoms in the Cu(111) Surface as Improved Catalytic Active Centers for Deoxygenation Reactions. *Catal. Sci. Technol*. **2021**, *14*, 4969-4978.
6. Cheng, N.; Zhang, L.; Doyle-Davis, K.; Sun, X. Single-Atom Catalysts: From Design to Application. *Electrochem. Energ. Rev.* **2019**, *2*, 539-573.
7. Manadé, M.; Viñes, F.; Illas, F. Transition Metal Adatoms on Graphene: A Systematic Density Functional Study. *Carbon,* **2015**, *95*, 525-534.
8. Kim, S.; Ruiz-Puigdollers, A.; Gamallo, P.; Viñes, F.; Lee, J.Y. Functionalization of γ-Graphyne by Transition Metal Adatoms. *Carbon*. **2014**, *120*, 63-70.
9. Khazaei, M.; Arai, M.; Sasaki, T.; Chung, C.; Venkataramanan, N.; Estili, M.; Kawazoe, Y. Novel Electronic and Magnetic Properties of Two-Dimensional Transition Metal Carbides and Nitrides. *Adv. Funct. Mater.* **2013**, *23*, 2185-2192.
10. Liu, Y.; Zhang, X.; Dong, S.; Ye, Z.; Wei, Y. Synthesis and Tribological Property of $Ti_3C_2T_x$ Nanosheets. *J. Mater. Sci*. **2017**, *52*, 2200-2209.
11. Zhang, X.; Lei, J.; Wu, D.; Zhao, X.; Jing, Y.; Zhou, Z. A Ti-Anchored Ti_2CO_2 Monolayer (MXene) as a Single-Atom Catalyst for CO Oxidation. *J. Mater. Chem. A*. **2016**, *4*, 4871-4876.
12. Zhang, C.; Cui, L.; Abdolhosseinzadeh, S.; Heier, J. Two-Dimensional MXenes for Lithium-Sulfur Batteries. *InfoMat.* **2020**, *2*, 613-638.
13. Gouveia, J.D.; Novell-Leruth, G.; Reis, P.; Viñes, F.; Illas, F.; Gomes, J.R.B. First-Principles Calculations on the Adsorption Behavior of Amino Acids on a Titanium Carbide MXene. *ACS Appl. Bio Mater*. **2020**, *3*, 5913-5921.
14. Gouveia, J.D.; Novell-Leruth, G.; Viñes, F.; Illas, F.; Gomes, J.R.B. The Ti_2CO_2 MXene as a Nucleobase 2D Sensor: A First-Principles Study. *Appl. Surf. Sci*. **2021**, *544*, 148946.
15. Vahidmohammadi, A.; Johanna, R.; Yuri, G. The World of Two-Dimensional Carbides and Nitrides (MXenes). *Science* **2021**, *372*, 6547.
16. Sholl, D.; Steckel, J.A. Density Functional Theory: A Practical Introduction. *Wiley Ed.* **2011**.
17. Born, M.; Oppenheimer, R. Zur Quantentheorie Der Molekeln. *Ann. Phys.* **1927**, *84*, 457-489.
18. Kohn, W.; Sham, L. J., Self-Consistent Equations Including Exchange and Correlation Effects. *Phys. Rev.* **1965**, *140*, A1133.
19. Capelle K. A Bird's-Eye View of Density-Functional Theory. *Braz. J. Phys*. **2002**, *36*, 1318–1343.
20. Přecechtělová, J.; Bahmann, H.; Kaupp, M.; Ernzerhof, M. Communication: A Non-Empirical Correlation Factor Model for the Exchange-Correlation Energy. *J. Chem. Phys*. **2014**, *141*, 111102.
21. Ortenzi, L.; Mazin, I.; Blaha, P.; Boeri, L. Accounting for Spin Fluctuations beyond Local Spin Density Approximation in the Density Functional Theory. *Phys. Rev. B.* **2012**, *86*, 064437.

22. Perdew, J.P.; Burke K.; Ernzerhof M. Generalized Gradient Approximation Made Simple. *Phys. Rev. Lett.* **1996**, *77*, 3865-3868.
23. Vega, L.; Viñes, F. Generalized Gradient Approximation Adjusted to Transition Metals Properties: Key Roles of Exchange and Local Spin Density. *J. Comput. Chem*. **2020**, *41*, 2598-2603.
24. Gábor, I.; Perdew, J.; Ruzsinszky, A.; Philipsen, P.; Lebègue, S.; Paier, J.; Vydrov, O.; Ángyán, J. Assessing the Performance of Recent Density Functionals for Bulk Solids. *Phys. Rev. B.* **2009**, *79*, 155107.
25. Muñoz-Galán, H.; Viñes, F.; Gebhardt, J.; Görling, A.; Illas, F. The Contact of Graphene with Ni(111) Surface: Description by Modern Dispersive Forces Approaches. *Theor. Chem. Acc*. **2016**, *135,* 165.
26. Viñes, F.; Gomes, J.R.B.; Illas, F. Understanding the Reactivity of Metallic Nanoparticles: Beyond the Extended Surface Model for Catalysis. *Chem. Soc. Rev.* **2014**, *43*, 4922-4939.
27. Yamamoto, N. Generalized Bloch Theorem and Chiral Transport Phenomena. *Phys. Rev. D*. **2015**, *92*, 085011.
28. Krotz, A.; Provazza, J.; Tempelaar, R. A Reciprocal-Space Formulation of Mixed Quantum–Classical Dynamics. *J. Chem. Phys.* **2021**, *154*, 224101.
29. Alhabeb, M.; Maleski, K.; Anasori, B.; Lelyuk, P.; Clark, L.; Sin, S.; Gogotsi, Y. Guidelines for Synthesis and Processing of 2D Titanium Carbide ($Ti_3C_2T_x$ MXene). *Chem. Mater.* **2017**, *29*, 7633-7644.
30. Hwu, H.H.; Chen, J.G. Surface Chemistry of Transition Metal Carbides. *Chem. Rev.* **2005**, *105*, 185-212.
31. Viñes, F.; Sousa, C. A Systematic Density Functional Theory Study of the Electronic Structure of Bulk and (001) Surface of Transition-Metals Carbides. *J. Chem. Phys*. **2005**, *122*, 174709.
32. Naguib, M.; Mochalin, V.N.; Barsoum, M.W.; Gogotsi, Y. 25th Anniversary Article: MXenes; A New Family of Two-Dimensional Materials. *Adv. Mater*. **2014**, *26*, 996-1005.
33. Anasori, B.; Lukatskaya R., M.; Gogotsi, Y. 2D Metal Carbides and Nitrides (MXenes) for Energy Storage. *Nat. Rev. Mater*. **2017**, *2*, 16098.
34. Keyhanian, M.; Farmazadeh, D.; Morales-García, Á.; Illas, F. Effect of Oxygen Termination on the Interaction of First Row Transition Metals with M_2C MXenes and the Feasibility of Single-Atom Catalysts. *Under Revision*.
35. Huang, B.; Neng, L.; Ong, W.J.; Zhou, N. Single Atom-Supported MXene: How Single-Atomic-Site Catalysts Tune the High Activity and Selectivity of Electrochemical Nitrogen Fixation. *J. Mater. Chem. A.* **2019**, *7*, 27620-27631.
36. Grimme, J.; Antony, J.; Ehrlich, S.; Krieg, H. A Consistent and Accurate *Ab Initio* Parametrization of Density Functional Dispersion Correction (DFT-D) for the 94 Elements H-Pu. *J. Chem. Phys*. **2010**, *132*, 154104.
37. Cheng, C.; Zhan, X.; Yang, Z.; Zhou, Z. Cu_3-Cluster-Doped Monolayer Mo_2CO_2 (MXene) as an Electron Reservoir for Catalyzing a CO Oxidation Reaction. *ACS Appl Mater. Interfaces* **2018**, *10*, 32903-32912.
38. Janthon, P.; Luo, S.; Kozlov, S.M.; Viñes, F.; Limtrakul, J.; Truhlar, D.; Illas, F. Bulk Properties of Transition Metals: A Challenge for the Design of Universal Density Functionals. *J. Chem. Theory Comput*. **2014**, *10*, 3882-3839.
39. Janthon, P.; Kozlov, S.M.; Viñes, F.; Limtrakul, J.; Illas, F. Establishing the Accuracy of Broadly Used Density Functionals in Describing Bulk Properties of Transition Metals. *J. Chem. Theory Comput.* **2013**, *9*, 1631-1640.
40. Yao, L.; Gu, Q.; Yu, X. Three-Dimensional MOFs@MXene Aerogel Composite Derived MXene Threaded Hollow Carbon Confined CoS Nanoparticles toward Advanced Alkali-Ion Batteries. *ACS Nano.* **2021**, *15*, 32238-3240.
41. Dolz, D.; Morales-García, Á.; Viñes, F.; Illas, F. Exfoliation Energy as a Descriptor of MXenes Synthesizability and Surface Chemical Activity. *Nanomaterials* **2021**, *11,* 127.
42. Wisesa, P.; McGill, K.A.; Mueller, T. Efficient Generation of Generalized Monkhorst-Pack Grids though the Use of Informatics. *Phys. Rev. B.* **2016**, *93*, 155109.